

# Uptakes and Images of $^{38}\text{K}$ in Rabbit Heart, Kidney, and Brain

Akira Takami, Katsuya Yoshida, Hiroyuki Tadokoro, Shinobu Kitsukawa, Kazuhiro Shimada, Mikio Sato, Kazutoshi Suzuki, Yoshiaki Masuda, and Shuji Tanada

Third Department of Internal Medicine, Chiba University School of Medicine, Chiba; and Division of Advanced Technology for Medical Imaging, National Institute of Radiological Sciences, Chiba, Japan

The purpose of this study was to evaluate the kinetics and image quality of positron-emitting  $^{38}\text{K}$  (half-life, 7.6 min) and high-resolution small-animal PET in the heart, kidney, and brain of rabbits. **Methods:** Studies were performed with 18 closed-chest anesthetized rabbits at baseline and during infusions of adenosine (0.2 mg/kg/min) and propranolol (0.5–1.0 mg/kg intravenously) using high-resolution small-animal PET.  $^{38}\text{K}$  was injected intravenously and dynamic PET imaging of the heart, kidney, or brain was performed for 3 min. Colored microspheres were injected into the left ventricle to measure organ blood flow. Arterial blood was withdrawn directly from the femoral artery, and, after the animals were killed,  $^{38}\text{K}$  activities in each organ were measured directly with a well counter. Uptake of  $^{38}\text{K}$  was calculated by dividing the  $^{38}\text{K}$  activities in each organ by the integral of the input function. The extraction fraction of  $^{38}\text{K}$  was estimated by dividing the uptake of  $^{38}\text{K}$  in each organ by the organ blood flow, measured by microspheres. **Results:** The left ventricular myocardium and kidney were clearly visualized, but there was no visual  $^{38}\text{K}$  uptake in the brain. For the heart, kidney, and brain, respectively, average blood flow was  $2.91 \pm 1.29$ ,  $5.49 \pm 0.71$ , and  $0.57 \pm 0.11$  mL/min/g, and the extraction fraction of  $^{38}\text{K}$  at baseline was  $0.55 \pm 0.13$ ,  $0.48 \pm 0.13$ , and  $0.022 \pm 0.004$ . The Renkin-Crone model fit the relation between myocardial extraction and flow under a wide range of myocardial blood flow ( $r = 0.89$ ). **Conclusion:**  $^{38}\text{K}$  is a suitable tracer for noninvasively showing the potassium kinetics of the heart, kidney, and brain by PET imaging.

**Key Words:**  $^{38}\text{K}$ ; PET; myocardium; kidney; brain

**J Nucl Med 2000; 41:763–769**

Among the many radionuclides of potassium analogs,  $^{201}\text{Tl}$  and  $^{82}\text{Rb}$  are widely used for cardiac SPECT and PET imaging to noninvasively assess myocardial perfusion and membrane integrity (1,2). Renal uptake of these tracers may also be used in the assessment of renal perfusion (3–5). However, brain uptake of potassium analogs is largely prevented by the blood–brain barrier (BBB) (6). Yet these tracers are useful for detecting breakdowns in the BBB, such as those caused by brain tumors or radiation injury (7).

Received Mar. 1, 1999; revision accepted Aug. 24, 1999.  
For correspondence or reprints contact: Katsuya Yoshida, MD, Third Department of Internal Medicine, Chiba University School of Medicine, 1-8-1 Inohana, Chuo-ku, Chiba, 260-8677, Japan.

Positron-emitting  $^{38}\text{K}$ , which has a half-life of 7.6 min, is a suitable tracer for investigating potassium kinetics in these organs. Although several experimental and clinical studies have reported on cardiac PET imaging (8–15), only a few reports have been published concerning  $^{38}\text{K}$  kinetics in the heart (13,14), none regarding the kidney, and 1 preliminary report on the brain (16). We recently developed a novel way of producing  $^{38}\text{K}$  (17) and a high-resolution cardiac PET system for imaging and quantitation of myocardial blood flow in rabbits (18). The purpose of this study was to evaluate the kinetics and image quality of  $^{38}\text{K}$  PET in the heart, kidney, and brain, based on our experimental procedures.

## MATERIALS AND METHODS

### Tracer Preparation

$^{38}\text{K}$  was obtained as a saline solution of  $^{38}\text{K}^+$  after the  $^{40}\text{Ar}(p,3n)^{38}\text{K}$  nuclear reaction. The target chamber (150 mm thick, 96 mL, 20 bar) was filled with pure argon gas and irradiated with 40 MeV of protons at a beam intensity of 6–6.5  $\mu\text{A}$  for 15 min. Immediately after the bombardment, irradiated gas was released through a 5-mL water reservoir to trap  $^{38}\text{K}$  in the gas phase. The water was then quickly introduced into the chamber, allowed to reflux for 1 min to recover  $^{38}\text{K}$  absorbed on the inner surface of the target chamber, and collected in a sterilized vial containing 45 mg NaCl through an anion exchange column and a 0.22  $\mu\text{m}$  Millex filter.  $^{38}\text{K}$  has a radionuclidic purity > 99.9%, which was determined by pure germanium detector. The chemical form of  $^{38}\text{K}$  was determined by using radio-ion chromatography as  $\text{K}^+$ . All procedures were previously described by Nagatsu et al. (17).

### Animal Preparation

Eighteen male Japanese white rabbits weighing 2.9–3.7 kg were studied. The animals were anesthetized with sodium pentobarbital (35 mg/kg) injected into the right marginal ear vein. The anesthetized state was maintained by a constant intravenous infusion of sodium pentobarbital at 6 mg/kg/h, beginning 1 h after induction. The rabbits were ventilated by tracheotomy using a small-animal ventilator (SN-480-5; Shinano, Tokyo, Japan). The settings of this ventilator and the oxygen content of inspired air were adjusted to maintain the blood gases in a physiologic range throughout the experimental period. Arterial blood samples were analyzed frequently for arterial  $\text{PaO}_2$ ,  $\text{PaCO}_2$ , and pH, with a Ciba-Corning pH/blood gas analyser (Model 238; Chiron Diagnostics, Emeryville, CA). The rabbits were paralyzed with pancuronium

bromide (0.3 mg/kg intravenously), with additional injections of 0.15 mg/kg intravenously every 30–40 min. Rectal body temperature was maintained at 38°C–39°C with a heating pad. Catheters were inserted into the right femoral artery for collection of microsphere reference samples and for obtaining arterial input function, into the left femoral artery for the measurement of blood pressure, and into the right jugular vein for the infusion of normal saline. For the injection of  $^{38}\text{K}$ , catheters were inserted into the left marginal ear vein for heart and kidney imaging. For brain imaging, we chose the femoral vein as the tracer injection site to avoid artifacts from the high tracer activities in the marginal ear vein to the brain image. The right carotid artery was cannulated for the injection of 15  $\mu\text{m}$  colored polystyrene microspheres (Dye-Trak; Triton Technology, Inc., San Diego, CA) through a polyethylene catheter (0.87 mm inside diameter, 1.27 mm outside diameter; Natume, Tokyo, Japan) advanced into the left ventricle. The animals were heparinized (400 U/kg) after the cannulations. Arterial pressures and heart rates were monitored with a multichannel polygraph (Omniace RT3200N; NEC San-ei, Tokyo, Japan). The rabbits were then placed in a supine position within the animal PET device. The experimental protocols for this study were approved by the Animal Welfare Committee of the National Institute of Radiological Sciences, Chiba, Japan.

## PET

PET images were obtained using a small-animal PET device (SHR-2000; Hamamatsu Photonics K.K., Hamamatsu, Japan) that provided 7 transaxial slices simultaneously. The slices had a transaxial resolution of 3.0 mm full width at half maximum (FWHM) and were separated by 6.5 mm. Axial resolution was 4.8 and 4.1 mm FWHM in direct and cross planes, respectively (19).

Initially, blank data for the correction of detection efficiency and the transmission data for tissue attenuation correction were collected using a  $^{68}\text{Ge}/^{68}\text{Ga}$  source. Subsequently,  $^{38}\text{K}$  was injected intravenously as a 20-s slow bolus into the marginal ear vein for heart and kidney imaging and into the femoral vein for brain imaging. The injection dose was 56–140, 83–140, and 182–222 MBq for heart, kidney, and brain, respectively. Simultaneously, an initial set of 6 10-s data frames was acquired, followed by 3 20-s and 2 30-s data. PET imaging (13 heart, 3 kidney, 3 brain) was performed for 3 min.

Because there was little visual uptake of  $^{38}\text{K}$  in the brain, we performed FDG PET studies on a rabbit after  $^{38}\text{K}$  brain PET imaging to clarify the position of the brain. FDG (186 MBq) injected intravenously at 12 min after the  $^{38}\text{K}$  injection, and, 50 min later, the data were collected over 10 min.

Each image was displayed as 180  $\times$  180 pixels with a pixel size of 1.0  $\times$  1.0 mm. Count losses at the high counting rates were corrected by single photon signals, because count losses on the PET scanner occur when single photon signals enter the photomultiplier or positron-encoding circuit. All reconstructions were performed without electrocardiographic gate and corrected for physical decay of the tracer.

## Experimental Protocols

Each rabbit was allowed to stabilize for 20–30 min after completion of the procedures. Approximately  $1.0 \times 10^6$  colored microspheres were dispersed with a mechanical mixer and then immediately injected into the left ventricle. Blood withdrawal began 15 s before the microsphere injection from the femoral artery at a constant rate of 1.5 mL/min to collect microspheres and obtain

arterial input function with BACC-4 (Hamamatsu Photonics K.K.). Immediately after the injection of microspheres,  $^{38}\text{K}$  was administered as a 20-s slow bolus while the imaging sequence began. PET images were then acquired. Blood sampling was stopped 2 min after the tracer injection. Low-molecular-weight dextran (mol wt 40,000; Otsuka Pharmaceutical Co. Ltd., Tokushima, Japan) was infused into the ear vein at a rate of 1.5 mL/min, concurrent with the withdrawal of the blood sample, to prevent any significant decrease in blood pressure during withdrawal. Intravenous infusions of adenosine and propranolol were given to obtain a wide range of myocardial blood flow. Eight rabbits were studied without any pharmacologic intervention. In 5 rabbits, myocardial hyperemia was induced with intravenous adenosine at a concentration of 0.2 mg/kg/min infused for 6 min. At 3 min after the start of adenosine infusion, microspheres and  $^{38}\text{K}$  were administered. To evaluate low flow, several doses of propranolol (0.5- to 1-mg/kg bolus intravenously) were injected into 5 rabbits. In total, 8 rest, 5 adenosine, and 5 propranolol experiments were performed in 18 rabbits. At 3 min after  $^{38}\text{K}$  injection, the animals were killed during deep anesthesia with KCl solution, and organs (heart, kidneys, and brain) were removed. The left ventricular myocardium, the right and left renal cortices, and the right and left cerebrums were dissected. The organs were weighed, counted in a well counter (Minaxi  $\gamma$ ; Packard Instrument, Downers Grove, IL), and corrected for radioactive decay.

The extraction of microspheres from blood and tissue samples was performed as described by Hale et al. (20). Regional blood flow was calculated from the equation:

$$\text{regional blood flow} = \text{Cm} \times \text{Qr/Cr}, \quad \text{Eq. 1}$$

where Cm is the total number of microspheres/g of myocardial tissue, Qr is the withdrawal rate of the reference blood sample (mL/min), and Cr is the total number of microspheres in the reference blood sample.

## Arterial Input Function

The high-efficiency bismuth germanate (BGO) coincidence detection system (BACC-4) was designed and built for applications in arterial blood sampling from small animals undergoing PET (18). The detection system uses 4 BGO detectors in a configuration to provide a small central opening with very high sensitivity for insertion of small-volume, flow-through blood-sampling tubing. Blood was withdrawn from the right femoral artery through the tubing at a constant flow (1.5 mL/min) with a Harvard pump (Model 11; Harvard Apparatus, Millis, MA), which allowed the simultaneous collection of colored microspheres. To calibrate this system to the well counter, serial blood samples were obtained from the ascending aortic catheter immediately after  $^{38}\text{K}$  intravenous injection in 5 rabbits under control conditions. A clipped catheter was placed within the ascending aorta through the right carotid artery. The clip was released to collect 2 or 3 drops of blood. From each blood sample, 250  $\mu\text{L}$  were then transferred to a test tube by micropipette. These samples then were measured with the well counter. Sampling intervals were 5 s during the first minute, every 10 s for the next minute, and every 20 s for the last minute. Arterial blood was also withdrawn from the femoral artery by Harvard pump and measured with the BACC-4. The dead volume from the femoral artery to BACC-4 was approximately 0.9 mL. The integral values of blood sampling data were compared with those determined with the BACC-4.

### <sup>38</sup>K Organ Uptakes

<sup>38</sup>K organ uptakes (extraction × flow) were calculated by the following equation:

$$E \times F = \frac{C_m(t)}{\int_0^t Ca(x)dx \times g}, \quad \text{Eq. 2}$$

where E is the extraction fraction of <sup>38</sup>K; F is the organ blood flow (mL/min/g); C<sub>m</sub>(t) and C<sub>a</sub>(t) are the <sup>38</sup>K activity concentrations in the organs and arterial blood, respectively, at time t; and g is the specific gravity of the organs (heart, 1.056 g/mL; kidney, 1.062 g/mL; and brain, 1.043 g/mL) (21). In this study, <sup>38</sup>K organ uptakes were calculated during the first 3 min of data acquisition (t = 3 min). Tracer concentrations in the organs were measured by well counter after the animals were killed. Arterial tracer concentrations were also measured with the BACC-4.

### Statistical Analysis

Hemodynamic data were expressed as mean ± SD. All data were analyzed by ANOVA. If a statistical significance was obtained, we used Scheffé's criteria for multiple comparison (22). A two-tailed P value < 0.05 was considered statistically significant.

## RESULTS

### Hemodynamics

The hemodynamics recorded at baseline and during the different pharmacologic interventions are summarized in Table 1. Compared with the control condition, adenosine caused a decrease in rate pressure product (RPP) (P = 0.097). Propranolol caused a significant decrease in systolic and diastolic blood pressure, heart rate, and RPP.

### Arterial Input Function

Figure 1A shows the time–activity curves of the arterial input function obtained with the well counter and BACC-4. The integral values obtained between 0 and 3 min and displayed in scatter plots between the results of the well

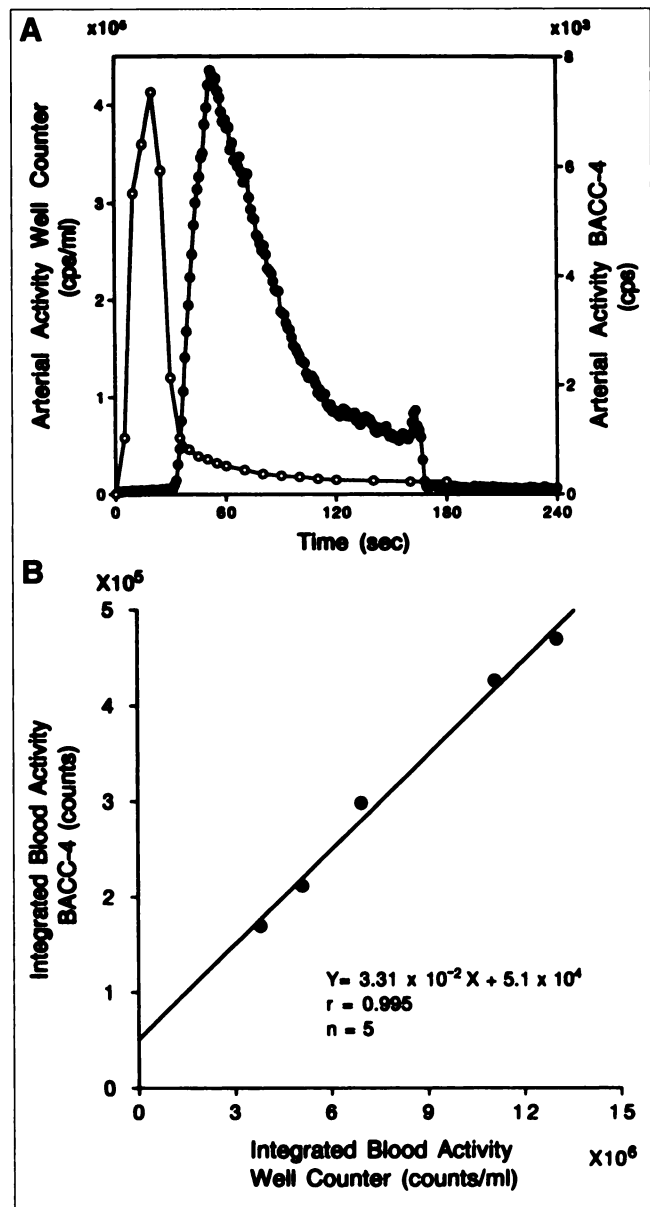


**FIGURE 1.** (A) Time–activity curves of arterial input function obtained by sampling directly from ascending aorta. ○ = well counter; ● = BACC-4. (B) Comparison of integral values of blood sampling data with those determined with BACC-4.

**TABLE 1**  
Summary of Hemodynamic Data During Pharmacologic Interventions

Intervention	Systolic BP (mm Hg)	Diastolic BP (mm Hg)	Heart rate (bpm)	RPP (mm Hg × bpm)
Control (n = 8)	129 ± 15	93 ± 13	308 ± 31	40,082 ± 7,788
Adenosine (n = 5)	126 ± 18*	80 ± 11	264 ± 59	32,090 ± 4,528*
Propranolol (n = 5)	92 ± 24†	67 ± 16†	236 ± 50†	21,017 ± 2,856†

\*P < 0.05 versus propranolol.

†P < 0.05 versus control.

BP = blood pressure; RPP = rate pressure product and was calculated as the product of systolic BP and heart rate. Values are mean ± SD.

counter and BACC-4 measurements are shown in Figure 1B. Although a time shift and dispersion of the arterial input function were observed with BACC-4 and not with serial sampling data, there was a good correlation between the integral values of serial sampling and BACC-4 data (r = 0.995).

### PET Imaging

Figure 2A shows typical serial images of the heart of 1 rabbit obtained after intravenous administration of <sup>38</sup>K at control condition. Good image quality was observed. At the midventricular level, the bolus transit through the blood pools and lungs was visualized during the first 30 s. Thereafter, the myocardial image was delineated. Figure 2B

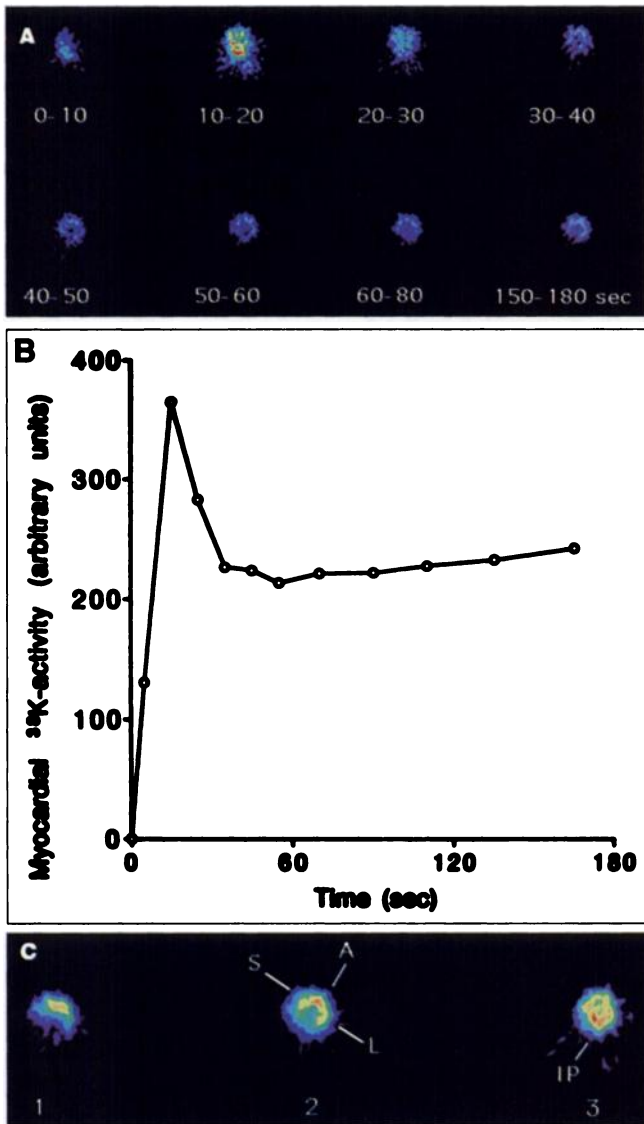


**FIGURE 2.** (A) Serial PET images obtained after intravenous injection of  $^{38}\text{K}$  at midventricular level in 1 rabbit. Lateral myocardium is on right; anterior is uppermost; and septum is on left. (B) Myocardial time–activity curve in same rabbit. (C) Three contiguous cross-sectional myocardial images obtained 2–3 min after administration of  $^{38}\text{K}$  in a rabbit under control condition. Uptake of tracer is homogeneous, and contrast between myocardium and both blood and lung is high. A = anterior; IP = inferoposterior; L = lateral; S = interventricular septum.

shows a typical time–activity curve of the myocardium from the myocardial region of interest (ROI) in the same rabbit in Figure 2A. Figure 2C shows 3 contiguous summed images of the left ventricular myocardium obtained 2–3 min after the administration of  $^{38}\text{K}$  in a control-condition rabbit. The myocardial image exhibited homogeneous accumulation of  $^{38}\text{K}$  activity.

Figure 3A shows a typical series of cross-sectional PET images of the left kidney of 1 rabbit, obtained after the intravenous administration of  $^{38}\text{K}$  under control conditions. The renal cortex was seen primarily during the first 30 s. Figure 3B is a typical time–activity curve of the kidney from

the renal cortical ROI in the same rabbit in Figure 3A. Figure 3C shows the summed images of the kidney obtained 2–3 min after the administration of  $^{38}\text{K}$  in a control-condition rabbit.  $^{38}\text{K}$  yielded high-quality PET images of the kidney.

Figure 4 shows the coronal images of the same normal rabbit brain obtained with  $^{38}\text{K}$  and FDG at control conditions. It shows summed images obtained 50–60 min after the administration of FDG, when the brain was clearly visualized. However, no visual  $^{38}\text{K}$  uptake was seen in the brain.

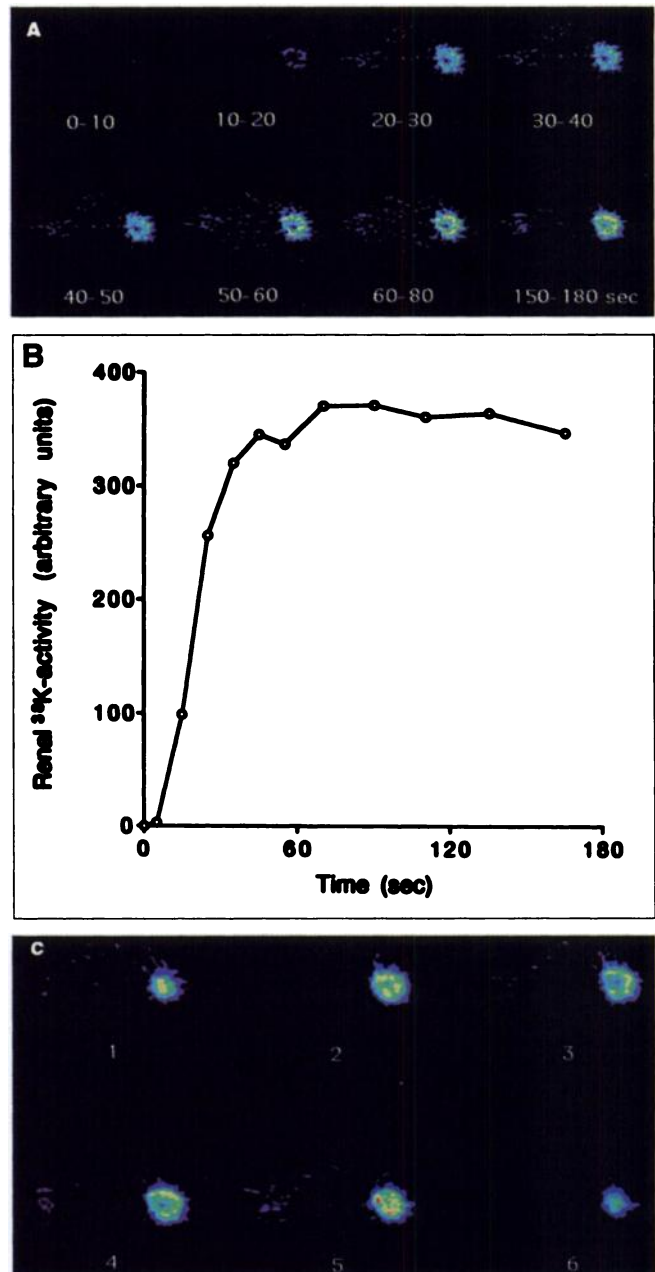


**FIGURE 3.** (A) Serial PET images obtained after intravenous injection with  $^{38}\text{K}$  at level of mid left of rabbit kidney. (B) Time–activity curve of same kidney. (C) Six contiguous cross-sectional images of kidney obtained 2–3 min after administration of  $^{38}\text{K}$  in a rabbit under control condition.

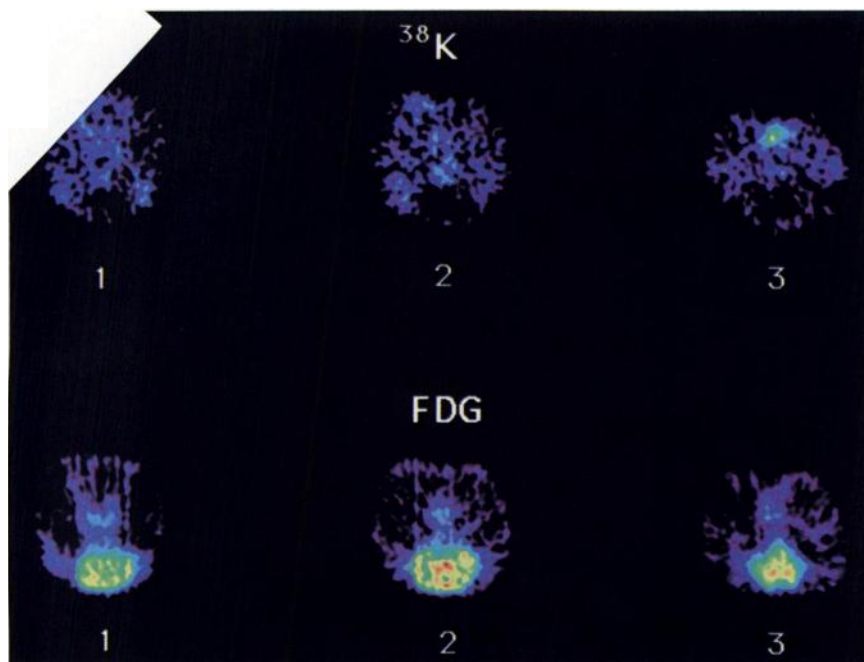


**FIGURE 4.** Comparison of coronal PET images of brain obtained with  $^{38}\text{K}$  and FDG in same rabbit. Note that brain images were clearly delineated by FDG PET (bottom row), but there was no visual uptake of  $^{38}\text{K}$  in brain (top row).

#### Comparison of $^{38}\text{K}$ Uptake with Blood Flow Measured with Microspheres

Table 2 shows  $^{38}\text{K}$  uptake in organs (mL/min/g), regional blood flow (mL/min/g) obtained with colored microspheres, and extraction fraction in the heart, kidney, and brain under control conditions.

Figure 5A shows the correlation between  $^{38}\text{K}$  myocardial uptake and myocardial blood flow measured simultaneously with microspheres. The curve shows that the relation is almost linear for flows <2.5–3.0 mL/min/g and that increases in flow lead to smaller changes in  $^{38}\text{K}$  uptake. Figure 5B shows the correlation between  $^{38}\text{K}$  myocardial extraction and flow. Applying the Renkin-Crone model (23,24) to the relation between  $^{38}\text{K}$  myocardial uptake and flow, the best equation fitting our data for the relation between them was:

$$U = F \times E = F \times (1 - e^{-2.4/F}) [r = 0.89]. \quad \text{Eq. 3}$$

The relationship between renal uptake of  $^{38}\text{K}$  and renal cortical blood flow under control conditions and with pharmacologic intervention is shown in Figure 6. Renal  $^{38}\text{K}$  uptake tends to rise as flow increases, although the points were slightly scattered compared with the relation between myocardial  $^{38}\text{K}$  uptake and flow. There was little uptake of

$^{38}\text{K}$  in the brain and this did not correlate with brain blood flow.

#### DISCUSSION

Since Sapirstein (25) described the fractionation distribution of indicators using  $^{42}\text{K}$ , the initial uptake of the isotopes of potassium analogs has been used as a marker of regional perfusion, particularly in the heart. We focused on the kinetics of the first 3 min after tracer injection to assess the feasibility of  $^{38}\text{K}$  as a PET imaging tracer in the heart, kidney, and brain. We estimated the quality of PET images and simultaneously measured the uptake and extraction of the tracer for these 3 organs. The results showed that the initial tracer uptake could be clearly visualized by dynamic PET in the heart and kidney. As expected, the uptake and extraction were high for both organs. Although brain uptake and extraction were extremely low because of the BBB, the possibilities offered by this technique in pathologic situations such as brain tumor and radiation necrosis indicate the need for further investigations.

The fitted curve (Fig. 5A) shows that the increase of myocardial  $^{38}\text{K}$  uptake was linear up to a flow of approximately 2.5–3.0 mL/min/g and then increased more gradually at high flows. The myocardial extraction fraction varied inversely with flow, and the Renkin-Crone model fit the relation between them (23,24). We have reported previously on the permeability  $\times$  surface area (the PS product) of  $^{13}\text{N}$ -ammonia in the heart in the same experimental preparation (18). The average value of  $^{13}\text{N}$ -ammonia, 2.7 mL/min/g, was slightly higher than that of  $^{38}\text{K}$ , probably because several percent of total ammonia is lipid-soluble  $\text{NH}_3$ . Bassingthwaite et al. (26) recently observed that the initial uptake of thallium exceeded that of potassium, interpreting this to mean that Na channels were certainly activated and

**TABLE 2**  
Regional Blood Flow, Uptake, and Extraction Fraction

Organ	Regional blood flow (mL/min/g)	Uptake (mL/min/g)	Extraction fraction
Heart	2.91 $\pm$ 1.29	1.50 $\pm$ 0.38	0.55 $\pm$ 0.13
Kidneys	5.49 $\pm$ 0.71	2.59 $\pm$ 0.64	0.48 $\pm$ 0.13
Brain	0.57 $\pm$ 0.11	0.012 $\pm$ 0.002	0.022 $\pm$ 0.004

account for much thallium transport compared with potassium. The comparison between the kinetics of potassium and its analogs is important. Additional experiments need to be performed using potassium analogs such as  $^{82}\text{Rb}$  and  $^{201}\text{Tl}$  in the same experimental preparation.  $^{38}\text{K}$  and PET may also be useful for the in vivo evaluation of the effects on myocardial potassium uptake under various pathophysiologic states affecting potassium channels and Na-K adenosine triphosphatase. The averaged myocardial blood flow at baseline in rabbits is reported to be 1.7–2.4 mL/min/g (27), which compares favorably with our data. However, these values are higher than those in dogs and humans, and care should be taken in applying the results of the rabbit studies to data from humans and dogs.

In this study, we measured cortical blood flow in the kidney, because it comprises 80%–90% of total renal blood flow (28). The flow values measured with microspheres in rabbits in this study are comparable with those in different animal species and human studies summarized by Nitzsche et al. (29). The averaged extraction fraction of  $^{38}\text{K}$  in the kidney measured at 0.48 is close to the value of 0.53 measured by Tamaki et al. (4) using dogs and  $^{82}\text{Rb}$  PET with a steady-state infusion model. Mullani et al. (5) reported that approximately 44.5% of the injected dose of  $^{82}\text{Rb}$  is excreted

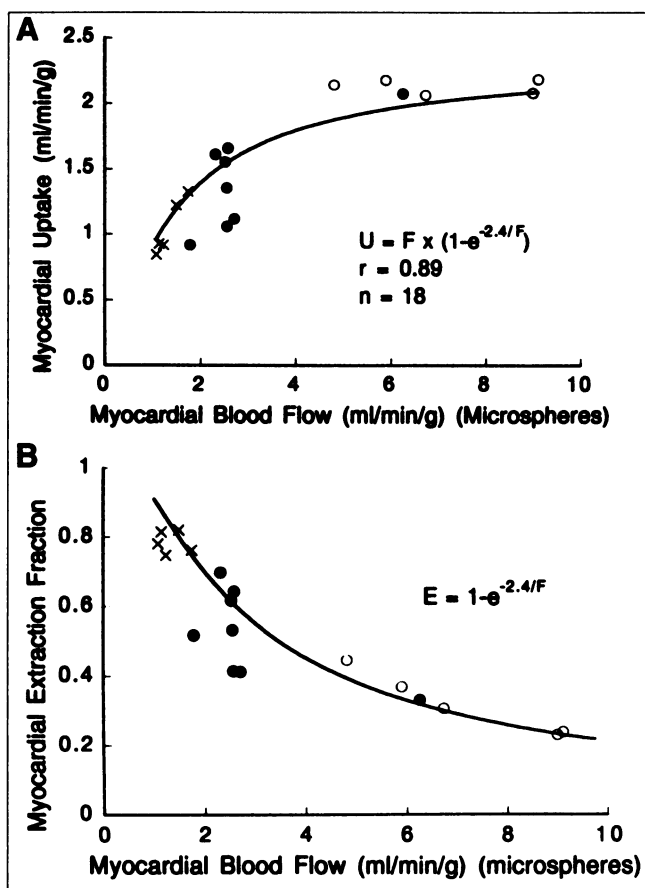


**FIGURE 5.** (A) Relationship between  $^{38}\text{K}$  myocardial uptake (extraction  $\times$  flow) and actual blood flow measured with microspheres.  $\circ$  = Adenosine;  $\bullet$  = controls;  $\times$  = propranolol. (B) Relationship between  $^{38}\text{K}$  myocardial extraction fraction and blood flow measured with microspheres.

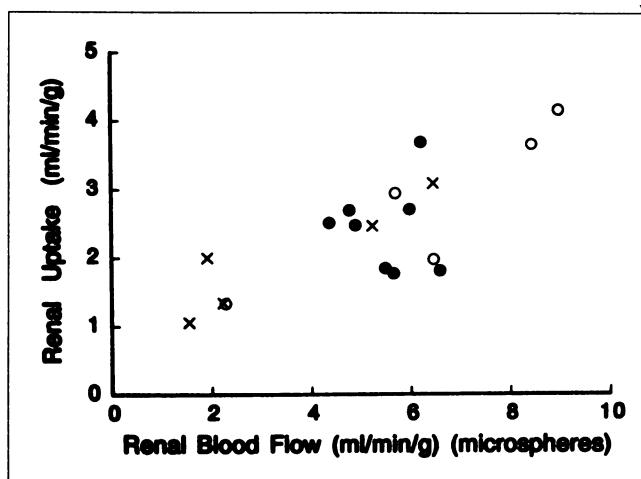


**FIGURE 6.** Relationship between  $^{38}\text{K}$  renal uptake (extraction  $\times$  flow) and actual blood flow measured with microspheres.

in the venous side and 9.75% in the ureter during the 150 s of data collection in a dog experiment. Thus, the extraction fraction is approximately 0.45, which represents an extraction fraction equivalent to that in our experimental preparation. Renal  $^{38}\text{K}$  uptake tends to rise as flow increases, although data were slightly scattered compared with the relation between myocardial  $^{38}\text{K}$  uptake and flow. In this study, adenosine and propranolol were chosen as pharmacologic interventions, mainly for assessing the  $^{38}\text{K}$  kinetics in the heart. In the kidney, however, renal blood flow is well controlled by autoregulation and does not increase remarkably above baseline. Additional studies need to be performed for a variety of pathophysiologic states related to decreased renal blood flow, such as renal artery stenosis, to investigate  $^{38}\text{K}$  kinetics in the kidney.

Potassium and its analogs cross the intact BBB slowly (6), so the initial uptake and extraction there were extremely low compared with those in the heart and kidney. Our mean baseline  $^{38}\text{K}$  extraction of 0.022 was close to the value of 0.021 measured by Brooks et al. (30) using  $^{82}\text{Rb}$  PET in humans, and the mean baseline  $^{38}\text{K}$  uptake of 12  $\mu\text{L}/\text{min}/\text{g}$  was higher than that estimated by direct quantification of  $^{86}\text{Rb}$  uptake in the brain from normal rats ( $3.5 \pm 0.3 \mu\text{L}/\text{min}/\text{g}$ ) as reported by Cserr et al. (31). Comparisons between the values should be carefully considered, as different species and experimental preparations were involved. Brain tumor uptake of potassium analogs was extremely high compared with that in the healthy brain and was a combined function of BBB permeability and cell viability.  $^{201}\text{Tl}$  is widely used for this purpose as a SPECT tracer (7).  $^{82}\text{Rb}$  also has the potential for this application (30,32–35). The kinetics of  $^{38}\text{K}$  in brain tumor should be investigated further.

## CONCLUSION

High-resolution PET for small animals was used to assess the potential capability of positron-emitting  $^{38}\text{K}$  for imaging

heart, kidney, and brain.  $^{38}\text{K}$  uptake was high for the heart and kidneys, and high-quality PET images were obtained 3 min after the tracer injection. Although  $^{38}\text{K}$  uptake in the brain was extremely low because of intact BBB, it might be useful for assessing BBB damage.  $^{38}\text{K}$  and PET would enable the noninvasive estimation of the kinetics of potassium in the heart, kidneys, and brain.

## ACKNOWLEDGMENTS

The authors thank Keiji Shimizu, Tsuyoshi Kosugi, and Hiroyuki Okada, Hamamatsu Photonics K.K., Hamamatsu, Japan, for their excellent assistance with PET imaging. They also thank Kotaro Nagatsu and Makoto Takei for preparing the  $^{38}\text{K}$ . This work was supported in part by the Japanese Special Coordination Fund for the Promotion of Science and Technology and by grants from the National Cardiovascular Center, Smoking Research Foundation, and Kashiwado Memorial Foundation of Japan.

## REFERENCES

- Bonow RO, Dilsizian V. Thallium-201 for assessment of myocardial viability. *Semin Nucl Med.* 1991;21:230-241.
- Gould KL. Clinical cardiac positron emission tomography: state of the art. *Circulation.* 1991;84: I22-I36.
- Hurwitz GA, Powe JE, Wesolowski CA, Mattar AG. Comparison of Tl-201 renal uptake with Tc-99m DTPA angiorenography in patients with hypertension. Measures of renal asymmetry. *Clin Nucl Med.* 1992;17:463-468.
- Tamaki N, Rabito CA, Alpert NM, et al. Serial analysis of renal blood flow by positron tomography with rubidium-82. *Am J Physiol.* 1986;251:H1024-H1030.
- Mullani NA, Ekas RD, Marani S, Kim EE, Gould KL. Feasibility of measuring first pass extraction and flow with rubidium-82 in the kidneys. *Am J Physiol Imaging.* 1990;5:133-140.
- Betz AL. Transport of ions across the blood-brain barrier. *Federation Proc.* 1986;45:2050-2054.
- Brunetti A, Alfano B, Soricelli A, et al. Functional characterization of brain tumors: an overview of the potential clinical value. *Nucl Med Biol.* 1996;23:699-715.
- Lambrecht RM, Hara T, Gallagher BM, Wolf AP, Ansari A, Atkins H. Cyclotron isotopes and radiopharmaceuticals-XXVIII. Production of potassium-38 for myocardial perfusion studies. *Int J Appl Radiat Isot.* 1978;29:667-671.
- Myers WG, Bigler RE, Graham MC. PET tomography in studies of distributions of 7.6-min potassium-38 in the dog heart. *Eur J Nucl Med.* 1984;9:272-277.
- Guillaume M, De Landsheere C, Rigo P, Czichosz R. Automated production of potassium-38 for the study of myocardial perfusion using positron emission tomography. *Appl Radiat Isot.* 1988;39:97-107.
- Duboc D, Kahan A, Maziere B, et al. The effect of nifedipine on myocardial perfusion and metabolism in systemic sclerosis. A positron emission tomography study. *Arthritis Rheum.* 1991;34:198-203.
- De Landsheere C, Mannheimer C, Habets A, et al. Effect of spinal cord stimulation on regional myocardial perfusion assessed by positron emission tomography. *Am J Cardiol.* 1992;69:1143-1149.
- Melon PG, Brihaye C, Degueldre C, et al. Myocardial kinetics of potassium-38 in humans and comparison with copper-62-PTSM. *J Nucl Med.* 1994;35:1116-1122.
- Bol A, Melin JA, Wijns M, et al. In vivo assessment of myocardial perfusion and viability by kinetics of potassium-38 [abstract]. *J Nucl Med.* 1994;35:77P.
- Melon PG, De Landsheere C, Degueldre C, Peters JL, Kulbertus HE, Pierard LC. Relation between contractile reserve and positron emission tomographic patterns of perfusion and glucose utilization in chronic ischemic left ventricular dysfunction. *J Am Coll Cardiol.* 1997;30:1651-1659.
- Duncan CC, Lambrecht RM, Bennett GW, Rescigno A, Ment LR. Observations of the dynamics of ionic potassium-38 in brain. *Stroke.* 1984;15:145-148.
- Nagatsu K, Kubodera A, Suzuki K. A novel way of producing an aqueous solution of  $^{38}\text{K}^+$  via the  $^{40}\text{Ar}(p,3n)$ -process. *Appl Radiat Isot.* 1998;49:1505-1510.
- Shimada K, Yoshida K, Tadokoro H, et al. High-resolution cardiac PET in rabbits: imaging and quantitation of myocardial blood flow. *J Nucl Med.* 1998;39:2022-2027.
- Watanabe M, Uchida H, Okada H, et al. A high resolution PET for animal studies. *IEEE Trans Med Imaging.* 1992;11:577-580.
- Hale SL, Alker KJ, Kloner RA. Evaluation of nonradioactive, colored microspheres for measurement of regional myocardial blood flow in dogs. *Circulation.* 1988;78:428-434.
- Webb AI, Weaver BM. Density of equine tissue at 37°C. *Res Vet Sci.* 1979;26:71-75.
- Wallenstein S, Zucker CL, Fleiss JL. Some statistical methods useful in circulation research. *Circ Res.* 1980;47:1-9.
- Renkin EM. Transport of potassium-42 from blood to tissue in isolated mammalian skeletal muscles. *Am J Physiol.* 1959;197:1205-1210.
- Crone C. The permeability of capillaries in various organs as determined by use of the indicator diffusion method. *Acta Physiol Scand.* 1963;58:292-305.
- Sapirstein LA. Regional blood flow by fractional distribution of indicators. *Am J Physiol.* 1958;193:161-168.
- Bassingthwaight JB, Winkler B, King RB. Potassium and thallium uptake in dog myocardium. *J Nucl Med.* 1997;38:264-274.
- Brewer NR, Cruise LJ. Physiology. In: Manning PJ, Ringler DH, Newcomer CE, eds. *The Biology of the Laboratory Rabbit.* 2nd ed. San Diego, CA: Academic Press; 1994:63-64.
- Knox FG, Spielman WS. Renal circulation. In: Shepherd JT, Abboud FM, eds. *Handbook of Physiology: The Cardiovascular System.* Bethesda, MD: American Physiologic Society; 1983:183-217.
- Nitzsche EU, Choi Y, Killion D, et al. Quantification and parametric imaging of renal cortical blood flow in vivo based on Patlak graphical analysis. *Kidney Int.* 1993;44:985-996.
- Brooks DJ, Beaney RP, Lammertsma AA, et al. Quantitative measurement of blood-brain barrier permeability using rubidium-82 and positron emission tomography. *J Cereb Blood Flow Metab.* 1984;4:535-545.
- Cserr HF, DePasquale M, Patlak CS. Volume regulatory influx of electrolytes from plasma to brain during acute hyperosmolarity. *Am J Physiol.* 1987;253:F530-F537.
- Valk PE, Budinger TF, Levin VA, Silver P, Gutin PH, Doyle WK. PET of malignant cerebral tumors after interstitial brachytherapy. Demonstration of metabolic activity and correlation with clinical outcome. *J Neurosurg.* 1988;69:830-838.
- Dhawan V, Jarden JO, Moeller JR, Strother SC, Rottenberg DA. Positron emission tomographic measurement of blood-to-brain and blood-to-tumour transport of  $^{82}\text{Rb}$ . II: clinical data and validation of technique. *Phys Med Biol.* 1989;34:1875-1794.
- Zunkeler B, Carson RE, Olson J, et al. Hyperosmolar blood-brain barrier disruption in baboons: an in vivo study using positron emission tomography and rubidium-82. *J Neurosurg.* 1996;84:494-502.
- Roedcke U, Radu EW, Hausmann O, Vontobel P, Maguire RP, Leenders KL. Tracer transport and metabolism in a patient with juvenile pilocytic astrocytoma. A PET study. *J Neurooncol.* 1998;36:279-283.